Geochemistry Geophysics Geosystems G3
AN ELECTRONIC JOURNAL OF THE EARTH SCIENCES
Published by AGU and the Geochemical Society

Article
Volume 5, Number 3
27 March 2004
Q03H10, doi:10.1029/2003GC000602
ISSN: 1525-2027

A detailed study of the polarity reversal mechanism in a numerical dynamo model

Johannes Wicht
Max Plank Institut für Aeronomie, Katlenburg-Lindau, Niedersachsen 37191, Germany (wicht@linmpi.mpg.de)

Peter Olson
Department of Earth and Planetary Sciences, Johns Hopkins University, Baltimore, Maryland 21218, USA (olson@jhu.edu)

[1] We analyze the mechanism of magnetic polarity reversals in a three- dimensional numerical dynamo model. A dynamo driven by compositional convection in a rotating spherical fluid shell with a solid, electrically conducting inner core exhibits regular reversals of its dominantly axial dipole magnetic field at Rayleigh number $Ra = 300$, Ekman number $E = 0.01$, Prandtl number $Pr = 1$ and Roberts number $q = 20$. The fluid motions that sustain the field include (1) azimuthal jets which generate toroidal magnetic field; (2) high-latitude, helical convective plumes which generate poloidal magnetic field; and (3) meridional circulation which transports the magnetic field. Inverse poloidal field is produced locally in the convective plumes. Outcrops of reversed field create inverse magnetic flux spots on the core-mantle boundary above the plumes that are precursors to the reversal. The dipole polarity change as seen from the surface occurs when the reversed magnetic flux is distributed over the core-mantle boundary by the meridional circulation. In our model, the reversed flux is transported from south to north and the transitional field has a strong quadrupole component. The duration of the dipole transition is the meridional transport time, and corresponds to a few thousand years in the Earth's core. The duration of the stable polarity epochs depends on several effects, including the strengths of the sources of normal and reversed poloidal field in the plumes, flux transport, and flux diffusion. Comparable reversal periods are found in an equivalent kinematic dynamo model with steady velocities and without Lorentz forces, confirming that these reversals are not triggered by changes in the flow and are primarily magnetic induction effects.

Components: 10,079 words, 12 figures, 1 table, 3 animations.

Keywords: Dynamo; magnetic field reversal; core convection; plumes; helicity.

Index Terms: 1535 Geomagnetism and Paleomagnetism: Reversals (process, timescale, magnetostratigraphy); 1510 Geomagnetism and Paleomagnetism: Dynamo theories; 1507 Geomagnetism and Paleomagnetism: Core processes (8115).

Received 18 July 2003; **Revised** 15 January 2004; **Accepted** 20 January 2004; **Published** 27 March 2004.

Wicht, J., and P. Olson (2004), A detailed study of the polarity reversal mechanism in a numerical dynamo model, *Geochem. Geophys. Geosyst.*, *5*, Q03H10, doi:10.1029/2003GC000602.

Theme: Geomagnetic Field Behavior Over the Past 5 Myr
Guest Editors: Cathy Constable and Catherine Johnson

1. Introduction

[2] Polarity reversals are a defining characteristic of the geomagnetic field, and an understanding of their cause is a central part of the geodynamo problem. There is now general agreement that reversals are caused by magnetohydrodynamic fluctuations within the core (rather than by external causes), a view supported by the many numerical dynamo models that reverse without the help of external disturbances [see *Kono and Roberts*, 2002]. Partly because polarity reversals can occur without external forcing, their true role in the geodynamo remains unclear. A traditional interpretation is that polarity reversals are infrequent and nearly random events [*Cox*, 1975; *Constable*, 2000, and references therein] implying that the geodynamo is rarely in a reversing configuration. The length of the major polarity epochs would seem to support this interpretation.

[3] However, the reversal process may actually be more regular and may occur far more frequently than the sequence of major polarity epochs would suggest. *Gubbins* [1999] has proposed that geomagnetic excursions should be interpreted as abbreviated reversals, which implies that the geodynamo is often in a reversing configuration. Records of recent excursions and reversals indicate that attempts of polarity changes occur with a characteristic frequency, approximately once in 20–40 kyr. This is about ten times more frequent than the traditional estimate, and implies that the associated dynamical mechanism occupies a far greater portion of the paleomagnetic record than is usually assumed. Numerical simulations by *Kutzner and Christensen* [2002] support the idea that reversals and excursions are manifestations of the same internal mechanism. Note, however, that *Gubbins* [1999] attributes the failure of reversal attempts to the long inner core diffusion time, while the model of *Kutzner and Christensen* [2002] has an insulating inner core. See the discussion on inner-core conductivity below.

[4] Evidence on reversals comes from a variety of sources. The sequence of the major polarity epochs is known from the magnetic record of the sea floor to approximately 160 Ma [*Harland et al.*, 1990]. Paleomagnetic studies provide some constraints on the duration of the polarity transitions and on the intensity and directional variations of the field during transition [*Jacobs*, 1984; *Merrill and McFadden*, 1999]. In addition, the observed secular variation of the geomagnetic field [*Bloxham et al.*, 1989; *Jackson et al.*, 2000] offers some clues to the reversal mechanism, even though the dipole polarity has not reversed in historical times.

[5] All of these observations have limitations for understanding the cause of reversals, because they pertain to the magnetic field at or near Earth's surface. These field measurements can be projected onto the core-mantle boundary to provide an image of the geodynamo on its outer surface. However, the magnetohydrodynamic processes that actually generate the magnetic field and cause polarity reversals are three-dimensional and operate within the volume of the core, possibly at depths far below the core-mantle boundary. Near-surface observations are additionally limited because they only detect the poloidal part of the core field. They do not detect the toroidal part of the core field, which plays an essential role in the geodynamo, including the polarity changes.

[6] In this paper we analyze the polarity reversal process in a numerical dynamo model. We identify the fluid dynamic mechanisms responsible for polarity change in a relatively simple but dynamically self-consistent dynamo model exhibiting repeated reversals that are regularly spaced in time. The sequence of events leading to polarity reversal in this model are described, and we show how these events appear in the magnetic field external to the core, and how they are related to the internal fluid dynamics. Although our model is very far from the Earth in parameter space, several of the critical steps in the reversal process appear to have analogs in the observed behavior of the geomagnetic and paleomagnetic fields. In addition, we relate some of the timescales that characterize the model polarity reversals, particularly the duration of the transition and the duration of uniform polarity epochs, to the fluid dynamical timescales of the dynamo. In section 2 we briefly

summarize some pertinent observational constraints on geomagnetic polarity reversals and review previous reversing dynamo model studies. In section 3 we describe the numerical dynamo model used in our study, and sections 4 and 5 analyze the reversals our model produces. We summarize our findings in section 6 and offer some interpretations of geomagnetic and paleomagnetic field behavior in light of our results.

2. Polarity Reversals

2.1. Paleomagnetic Reversals

[7] Most of the time the Earth's field is dominated by a geocentric axial dipole component, with normal and reversed polarities represented in essentially equal portions. Polarity reversals are the transitions between these two states. Excursions are possibly related phenomena. During an excursion the field departs substantially from a geocentric axial dipole for a few thousand years, then returns to its original polarity [*Merrill et al.*, 1996].

[8] The attributes common to most polarity reversals, as inferred from a large number of paleomagnetic studies, have been summarized recently by *Merrill and McFadden* [1999] and *Dormy et al.* [2000]. Because of genuine differences between individual reversals, and also because of difficulties in obtaining reliable spatial and temporal coverage, several of these attributes remain controversial or poorly documented. The characteristics that are best agreed on include the following. The major polarity epochs have variable duration. The average duration of the major epochs (polarity chrons) during the last 10 Ma is 0.2–0.25 Myr, but the present Brunhes epoch lasts already 0.79 Myr [*Cande and Kent*, 1995]. Long-term trends in polarity epoch length are best exemplified by the 36 Myr Cretaceous superchron, which suggest an influence of the mantle on the geodynamo. There is little evidence for polarity bias, implying that normal and reversed fields have the same average structure and are equally probable. On the basis of virtual dipole interpretations of paleomagnetic sequences the duration of field reversals is estimated to be about 5 kyr. The magnetic field intensity is reduced prior to and during the polarity transition, typically by a factor 2–10, but the field recovers quickly (usually within a few kyr) without dwelling in a low intensity state. Transition magnetic fields include nondipole components but retains some large-scale structure, since VGP (virtual geomagnetic pole) paths are usually seen to cross the equator abruptly along nearly meridional trajectories.

[9] We mention two other potentially important attributes of reversals, which are not so well established. First, there is evidence that the major polarity epochs include multiple short polarity epochs and frequent magnetic excursions. Overall these may be ten times more frequent than the reversals that separate the major chrons [*Langereis et al.*, 1997]. The shorter events possibly constitute a better definition of the true reversal timescales in the core, since they may be more regular than the major epochs. Second, there is some evidence of "sawtooth" intensity variations during polarity epochs, where the intensity is highest shortly after polarity change and tends to decrease prior to the next reversal [*Valet and Meynadier*, 1993]. These two attributes suggest a different interpretation of the underlying processes. They may be much more frequent than the rarity of consolidated polarity changes suggests, the processes may also be partly deterministic, perhaps even cyclical. Periodic behavior is seen in theoretical dynamo models [*Moffat*, 1978] and in the solar dynamo, as evidenced by the sunspot cycle. The geodynamo appears to be less regular than the solar dynamo, but perhaps this is because the characteristic frequencies of dynamo processes are much lower in the core than in the sun. In view of the fundamental uncertainties in interpreting the paleomagnetic reversal record, numerical models can play a useful role, by identifying sources of periodic and random behavior in the geodynamo.

2.2. Evidence From Geomagnetic Secular Variation

[10] Although the geomagnetic field in historical times is dominated by a stable axial dipole, there are some characteristics of its secular variation that may bear on the polarity reversal mechanism. Foremost among these are reversed flux spots at

middle and high latitudes on the core-mantle boundary. There are several regions on the core-mantle boundary where the magnetic field direction is locally reversed [*Bloxham et al.*, 1989]. The largest concentration is beneath the South Atlantic, where a group of reversed flux spots extend from South Africa to South America. Other reversed flux spots occur at high latitudes within the northern hemisphere inner core tangent cylinder, where a purely geocentric axial dipole would have maximum intensity. In addition, comparison of the 1980 Magsat and 2000 Oersted core field models reveals several new reversed flux spots in early stages of formation [*Hulot et al.*, 2002] including one beneath the Western Atlantic near Bermuda.

[11] A related phenomenon is the decay of the geocentric axial dipole, presently at a rate of $-0.06\%\ \mathrm{yr}^{-1}$. The current rate of decay of the axial dipole, equivalent to an exponential decay time of 1600 yrs, is about 15 times faster than free decay of the fundamental mode dipole field, assuming an electrical conductivity of $6 \times 10^5\ \mathrm{S\ m}^{-1}$ for the outer core [*Secco and Schloessin*, 1989]. This accelerated decay is mainly due to growth and poleward motion of the reversed magnetic flux spots, particularly those in the southern hemisphere [*Gubbins*, 1987]. Rapid growth and poleward motion of reversed flux spots is an efficient way to change the polarity of the external dipole field, and is in fact the surface expression of the reversal mechanism in our dynamo model.

2.3. Polarity Reversals in Numerical Dynamo Models

[12] A growing number of self-consistent, three-dimensional dynamo models have recurring polarity reversals. *Glatzmaier and Roberts* [1995] were the first to report several polarity reversals in a self-consistent three-dimensional dynamo model. This particular dynamo model was highly chaotic and the polarity reversals occurred at irregular intervals. Later, *Kida et al.* [1997] produced regular (nearly periodic) reversals in a three-dimensional dynamo model. A study by *Sarson and Jones* [1999] reported reversals in a dynamo model with low azimuthal resolution, and attributed the reversals to fluctuations in the strength of a polar upwelling plume. We highlight this study in particular because it identifies plume upwellings as the critical fluid dynamic element in the reversal, in accord with our results.

[13] One important objective in dynamo modeling is to identify the parameters that control reversal frequency. Since all numerical dynamos are far from the geodynamo in terms of their input parameters, most of the focus in model studies has been on the relative (rather than absolute) reversal frequency. It is now established that reversal frequency depends on boundary conditions, especially boundary heterogeneity, and even more sensitively on the Rayleigh number of the convection.

[14] In a comparison of dynamos with different patterns of boundary heat flow heterogeneity, *Glatzmaier et al.* [1999] showed that patterns with axial and equatorial symmetry plus an increased heat flux above the poles tend to produced larger magnetic secular variation and more frequent reversals. A possible reason is that these configurations are compatible with the long-time average convective heat flux that develops when a homogenous boundary temperature is assumed instead. This 'natural' heat flux was at least partly opposed by those heterogeneous conditions that led to smaller secular variation and fewer reversals.

[15] *Coe et al.* [2000] analyzed the external field from several of these reversals in detail, and concluded that some were comparable with geomagnetic reversals as inferred from the paleomagnetic record. However, they also found that more than one type of reversal was present in these models, and not all of them were ''Earth-like''. In particular, some of the reversals involved long-lived, nondipolar transitional states, which do not appear to have paleomagnetic counterparts. The fact that many dynamo models use hyperdiffusivity (scale-dependent diffusion) to ensure numerical stability begs the question whether the reversal frequency in such dynamo models depends on this particular parameterization. It seems that hyperdiffusivity does influence polarity reversals [*Grote and Busse*, 2000]. However, existence of

reversals in three-dimensional dynamo models without hyperdiffusivity is now well established [*Kageyama et al.*, 1999; *Kutzner and Christensen*, 2002; *Wicht*, 2002].

[16] *Kutzner and Christensen* [2002] explored the dependence of reversal rate on Rayleigh number and convective forcing (internal versus boundary-derived buoyancy sources), deliberately avoiding the use of hyperdiffusivities. They found that the Rayleigh number has the greatest control on secular variation and also reversal frequency. With increasing Rayleigh number (holding the Ekman number, i.e., the rotation rate, constant), the dynamo behavior changes from a nonreversing state, with low secular variation and dominant axial dipole, to another configuration. The magnetic field in this second configuration is more variable in time and is not dominated by the dipole component any more. *Kutzner and Christensen* [2002] showed there exists an intermediate regime in which the dynamo switches between these two states, the switches being polarity reversals. For some cases in this intermediate regime the reversals were abrupt, as in the paleomagnetic record, while for other cases the reversals occurred within long-lived, nondipolar transitional field states.

[17] The presence of the solid inner core may have an important effect on polarity reversals. *Hollerbach and Jones* [1993] have claimed that electrical conduction in the solid inner core can reduce the frequency of magnetic field reversals, by Ohmic damping of high-frequency components of geomagnetic secular variation. Their interpretation was based on the behavior of reversals in a heavily parameterized mean-field dynamo model. The effect of electrical conductivity in the inner core on reversal frequency in fully three-dimensional dynamos was investigated by *Wicht* [2002]. He found that inner core conductivity reduces the probability of very short polarity epochs, those with lengths in the order of 1000 years. However, *Wicht* [2002] found no significant influence of the inner-core conductivity on the probability of polarity epochs of 10,000 years or longer, because the dipole field has time to recover from low values associated with the reversal process.

[18] The main objectives of previous studies have been to determine the sensitivity of reversal frequency to model parameters and the geometry of the external field during transition, with relatively little attention given to the mechanisms that cause the reversals. This is particularly true for the highly chaotic dynamo models, where the magnetic field and the flow have spatial and temporal complexity, and the mechanisms driving the reversal are difficult to isolate. Our approach is to restrict attention to a relatively simple dynamo model, one with a regular reversal cycle. We examine the cycle of reversals using three-dimensional time-dependent images, and we relate the behavior of the external field during polarity reversal to the dynamical processes in the interior of the dynamo.

3. Dynamo Model

3.1. Governing Equations

[19] The important elements of our dynamo model have been described previously [*Christensen et al.*, 1999; *Wicht*, 2002]. We model three-dimensional, time-dependent convection and magnetic field generation in a rotating sphere. The outer shell of the sphere is filled with an electrically conducting, Boussinesq fluid representing Earth's liquid outer core. The central sphere is solid with the same electrical conductivity as the fluid, and represents Earth's inner core.

[20] We solve the Navier-Stokes equation with full inertia, Coriolis, and Lorentz forces, and uniform Newtonian viscosity, coupled to the buoyancy transport equation and the magnetic induction equation in a spherical coordinate system (r, θ, ϕ) rotating with uniform angular velocity $\Omega\hat{\mathbf{z}}$ about the z-axis. In dimensionless form the governing equations are:

$$\frac{E}{q\,Pr}\left(\frac{\partial \mathbf{u}}{\partial t}+\mathbf{u}\cdot\nabla\mathbf{u}\right)-E\,\nabla^2\mathbf{u}+2\,\hat{\mathbf{z}}\times\mathbf{u}= -\nabla P+Ra\,q\,Pr\,\hat{\mathbf{r}}\,\frac{r}{r_o}\,T+(\nabla\times\mathbf{B})\times\mathbf{B} \tag{1}$$

$$\nabla\cdot\mathbf{u}=0 \tag{2}$$

$$\frac{\partial T}{\partial t}+\mathbf{u}\cdot\nabla T=Pr^{-1}\left(\nabla^2 T-1\right) \tag{3}$$

$$\frac{\partial \mathbf{B}}{\partial t}=\nabla\times(\mathbf{u}\times\mathbf{B})+\nabla^2\mathbf{B} \tag{4}$$

where **B**, **u**, P and T are magnetic induction, velocity, pressure perturbation and buoyancy variable, respectively, and $\hat{\mathbf{r}}$ is the radial unit vector. The buoyancy variable models the relative amount of light elements that are released due to inner core freezing. The term -1 on the left hand side of the buoyancy equation represents volumetric sinks that balance the fixed buoyancy flux through the inner-core boundary. The flux through the outer boundary is set to zero. We use the volumetric sink density ϵ to scale the buoyancy variable T with $[\epsilon D^2/\kappa]$. Here, κ is the buoyancy diffusivity (chemical diffusivity of light elements) and D the shell thickness, which is used as the basic length scale. In order to match the geometry of Earth's core, we set the dimensionless outer radius r_o = 1.5398 and the inner radius r_i = 0.5398, so that $D = r_o - r_i = 1$. The magnetic field intensity is scaled by $(\rho\mu\eta\Omega)^{1/2}$, with ρ the density, μ the magnetic permeability and η the magnetic diffusivity. Time in the calculation is measured in the magnetic diffusion time $t_\eta = D^2/\eta$.

[21] Our model includes four dimensionless input parameters. These are the Ekman number $E = \nu/\Omega D^2$, the Prandtl number $Pr = \nu/\kappa$, the (modified) Rayleigh number $Ra = \alpha g_o \epsilon D^3/\nu\kappa\Omega$ and the Roberts number $q = \kappa/\eta$, where α is a compositional expansivity, and g_o is gravity at the outer boundary. There are two important output parameters, one for the magnetic field intensity, the other for fluid velocity. The dimensionless magnetic field intensity is given in units of $\sqrt{\Lambda}$, where, in terms of dimensional magnetic field $\tilde{B}$, $\Lambda = \tilde{B}^2/(\rho\mu\eta\Omega)$ is the Elsasser number. Dimensionless fluid velocities are given in units of the magnetic Reynolds number $Rm = \tilde{U}D/\eta$, where $\tilde{U}$ is the dimensional fluid velocity.

[22] We assume that both spherical boundaries are rigid and impermeable. The outer boundary is electrically insulating, while the inner core is electrically conducting (with the same conductivity as the fluid), and is free to rotate under the action of applied mechanical and electromagnetic torques [*Wicht*, 2002].

3.2. Numerical Technique

[23] The magnetic field is represented in terms of poloidal and toroidal parts according to

$$\mathbf{B} = \mathbf{B}(poloidal) + \mathbf{B}(toroidal) = \nabla \times \nabla \times \hat{\mathbf{r}} P + \nabla \times \hat{\mathbf{r}} T \tag{5}$$

[24] We use the basic pseudo-spectral method described in *Glatzmaier* [1984] to solve equations (1)– (4). Time stepping is a mixed implicit/explicit scheme. The Coriolis force and nonlinear terms are calculated in grid space and treated explicitly. The implicitly handled linear terms are evaluated in spectral space, using Chebychev polynomials in the radial direction and spherical harmonics in the horizontal directions. The maximum Chebychev polynomial degree and the maximum degree and order of the spherical harmonics are N = 30 and L = 42, respectively. The associated numbers of grid points are 33 in radial direction, 64 in meridional direction, and 128 in azimuthal direction. Spherical transforms are alias-free. Simple convergence tests have revealed that the resolution is sufficient. The spectral method uses fast Fourier transforms in azimuthal direction and Gauss-Legendre integration to transform between latitudinal grid points and spherical harmonics as has been described previously [*Glatzmaier*, 1984]. A similar method is used to transform between radial grid points and Chebychev polynomials.

[25] The inner-core field is supported at 13 grid points using the method described in *Wicht* [2002]. It is free to rotate relative to the liquid outer core about the polar axis, subject to the combined action of Lorentz and viscous torques. Details of the inner core torque calculation are given in *Wicht* [2002].

4. Reversals in a Dynamic Dynamo Model

4.1. The Model

[26] We have selected a model with moderate parameter values: (modified) Rayleigh number Ra = 300, Ekman number E = 0.01, Prandtl number Pr = 1, and Roberts number q = 20. The Rayleigh number is about 7.5 times supercritical for the onset of (nonmagnetic) convection. In particular the high Ekman number allows for a convective flow that is significantly nongeostrophic and in this respect differs from the anticipated conditions in the Earth outer core and from the configuration in many

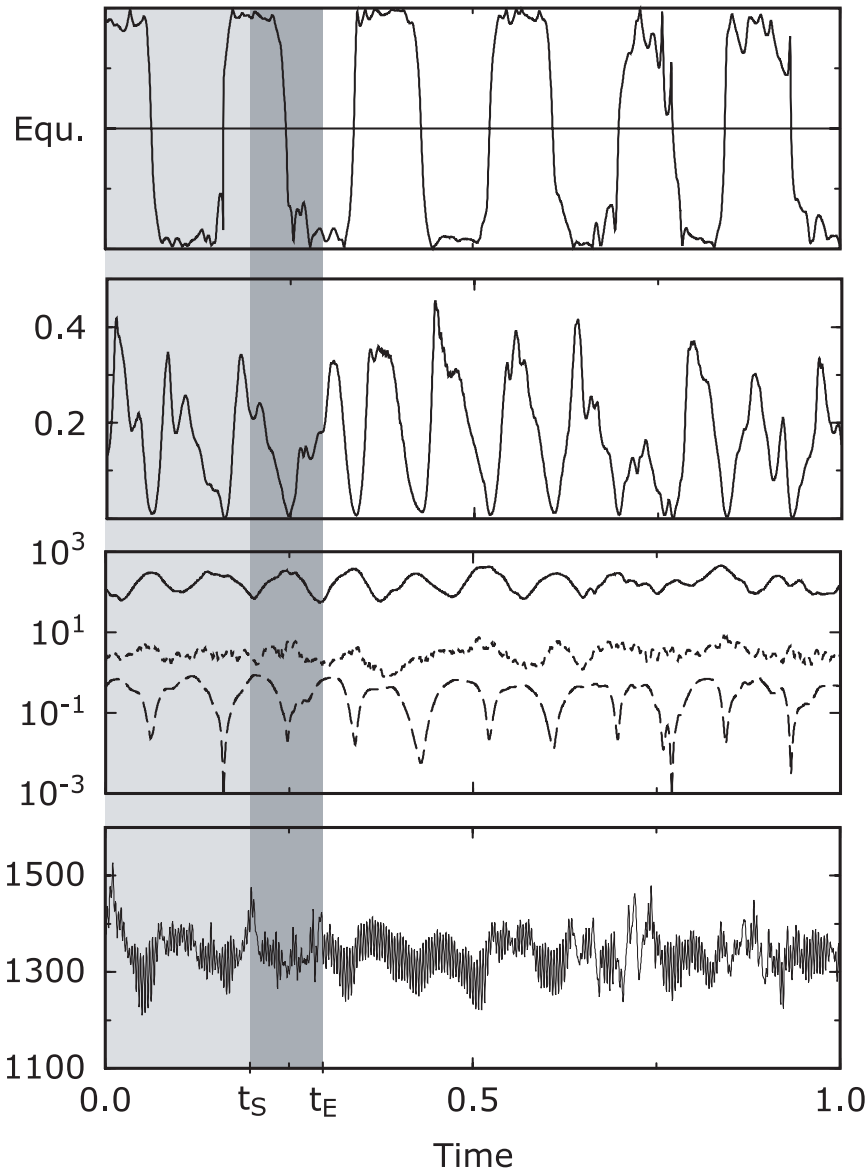

Figure 1. Time series of the dynamo model over several polarity epochs. The time scale is given in magnetic diffusion time units $t_\eta = D^2/\eta$. First panel shows the dipole polarity function (Latitude of dipole at CMB); second panel shows relative contribution of the magnetic dipole to the total magnetic energy at the CMB; third panel shows total magnetic energy in the outer core (solid line), total dipole energy in the outer core (dotted line), and total dipole energy at the CMB (dashed line); fourth panel shows total kinetic energy. The dark gray shaded time span is depicted as a standard reversal epoch in most of the analysis presented here, the light gray shaded span is shown in 2-D animations.

other dynamo simulations. We discuss the differences in more detail below.

[27] Figure 1 shows time sequences of key properties during one magnetic diffusion time. Time averaged Elsasser number and magnetic Reynolds number for this run are $\Lambda = 4.8$ and $Rm = 250$, quite similar to Earth's values. The upper panel in Figure 1 displays the polarity function, the colatitude of the magnetic dipole at the core-mantle boundary (CMB). The time behavior is somewhat chaotic but the reversals occur regularly in a periodic fashion and always obey very similar dynamics. In particular, the record shows short periods of dipole transitions separated by longer intervals of stable polarity.

[28] Eleven polarity reversals are present in Figure 1. The dimensionless time unit is the magnetic diffusion time $D^2\sigma\mu$. Assuming an electrical conductivity of $\sigma = 5 \times 10^5$ S m^{-1} such a time unit would represent 200,000 years for the geomagnetic field. The average time between successive reversals, equivalent to the average polarity epoch length, is 0.09 in dimensionless units, approximately 18,000 years in the core. This time is too short by a factor 10–15 compared to the average length of polarity chrons in recent paleomagnetic reversal records [*Merrill et al.*, 1996]. However, it is more comparable to the average time between excursions in the recent past, as argued by *Gubbins* [1999].

[29] The duration of the model reversals, defined as the time for the polarity function to pass between two latitudes, (between ±45°, for example) is comparable to reversals of the Earth's field. Although somewhat variable, the polarity function shown in Figure 1 changes by 90° of latitude within 0.01 time units on average, equivalent to about 2000 years in the Earth. This is within the range of the paleomagnetic estimates for the time required for the VGP (virtual geomagnetic pole) to move by 90° of latitude during a reversal [*Merrill and McFadden*, 1999].

[30] The relative contribution of the dipole to the total magnetic field energy at the CMB reaches its maximum quickly after a reversal and slowly decays toward the next polarity change, as shown in the second panel of Figure 1. However, the third panel in Figure 1 demonstrates that the total magnetic energy increases during the reversal as does the dipole energy in the core. Only the dipole at the CMB is decreasing due to the particular dynamics of the reversals. Panel 4 in Figure 1 shows the kinetic energy, a closer analysis of its time behavior is presented in section 5. Gray shaded areas in Figure 1 represent the time spans that are depicted by illustrations and animations presented below. Light gray shaded times are covered by two-dimensional (2-D) animations in Animation 1. The time span shaded in dark gray has been chosen as a standard reversal period here. We will present it in three-dimensional (3-D) Animations 2 and 3 and illustrate the solutions at start $t = t_S$ and end $t = t_E$ of this period with several figures below.

4.2. Convective and Magnetic Fields

[31] The main convective structures at t_S are shown in Figure 2. They include an upwelling polar plume in the northern hemisphere and two mid-latitude upwelling plumes in the southern hemisphere. Figure 2a displays the radial convective buoyancy flux to illustrate this configuration. The orientation of the southern plumes is intermediate between radial (parallel to $\hat{\mathbf{r}}$) and axial (parallel to $\hat{\mathbf{z}}$), reflecting the moderate influence of rotation in this calculation. These plumes originate at the inner boundary near 40°S latitude and reach the outer boundary near 55°S latitude. Although as many as four upwelling plumes are present at times in the southern hemisphere, they do not all appear to play a major role in this dynamo, because $m = 2$ always remains the dominant nonaxisymmetric wavenumber in the convective field. The primary locations of downwellings are at the southern pole and along the inner core tangent cylinder in the northern hemisphere, which corresponds to about 65°N latitude at the outer boundary.

[32] This general pattern of upwelling plumes and downward return flows results in the pattern of azimuthally averaged meridional circulation shown in the right hemisphere of Figure 2b. Flow in the large meridional cell outside of the inner core tangent cylinder is northward near the outer boundary and southward deeper in the shell. This circulation plays a crucial role in the reversal process and governs the duration of the dipole polarity transition. In addition, there are meridional cells at high latitudes in both hemispheres. Because these cells are smaller and are confined within the inner core tangent cylinder, they play subordinate roles in the reversal process. Planetary rotation interacts with the main meridional cell, producing strong azimuthal jets in each hemisphere. As shown in the left hemisphere of Figure 2b, the northern hemispheric jet is prograde (eastward) whereas the jet in the southern hemisphere flows retrograde (westward).

[33] Figure 3 compares the radial magnetic fields at start t_S and end t_E of the standard reversal period at

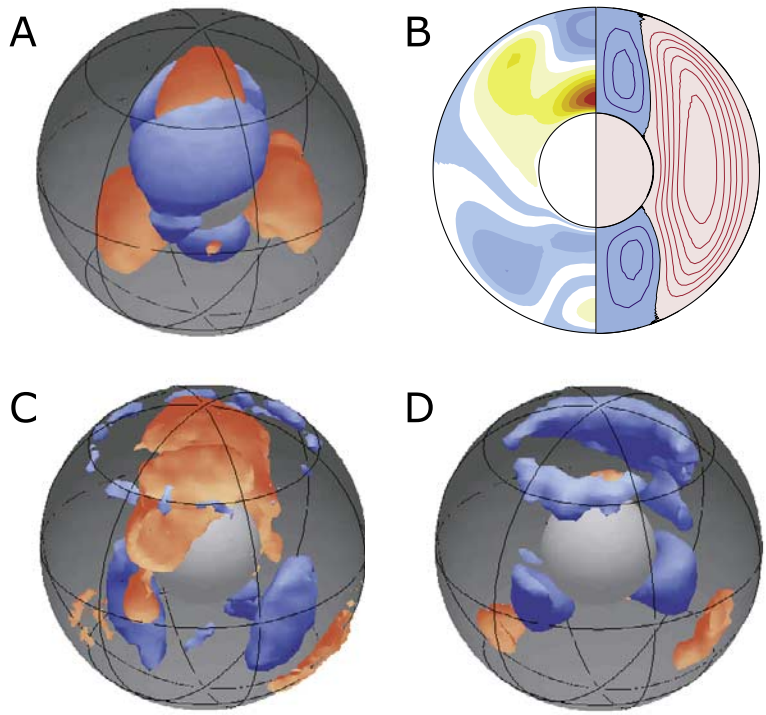

Figure 2. Snapshot images of the convection in the reversing dynamo model. (a) Isosurfaces of the radial convective buoyancy transport, red represents outward and blue inward transport with about 10% of the absolute amplitudes; (b) Zonal averaged rotation rate at left (contour interval = 2.7×10^4deg/t_η) and streamlines of meridional flow at right; (c) Isosurface of the z-vorticity, positive in red and negative in blue at 27% of the absolute maximum; (d) Isosurfaces of positive (red) and negative (blue) helicity at 19% of the absolute maximum.

a radial level equivalent to the Earth's surface, and at the external boundary of the model representing the core-mantle boundary (CMB). The 'surface' field is dominated by the dipole contribution, but the CMB field shows significant differences between the structures in the northern and southern hemispheres. Field is concentrated at the south pole by the downwelling there, field is also concentrated by the tangent cylinder downwellings in the northern hemisphere. Patches with minimal or reversed flux are present at high latitudes in each hemisphere. These patches are located over (or closely adjacent to) two upwelling plumes. A local minimum in the radial field occurs above the northern upwelling.

[34] Three kinematic properties of the plumes are especially significant for this dynamo. The first is azimuthal drift. The southern plumes drift to the west at a rate of roughly 2.0×10^4 degrees per magnetic diffusion time, and are located within the azimuthal retrograde jet. In contrast, the nonaxisymmetric part of the convective structure in the northern hemisphere drifts to the east, at about 2.6×10^4 degrees per magnetic diffusion time. These azimuthal drifts represent the dominant source of time dependence in the convective flow. Shearing of poloidal magnetic field by gradients in the aimuthal flow is the main source for toroidal magnetic field.

[35] Another significant property is helicity, the correlation of velocity and vorticity in the plumes. Snapshots of the z-vorticity and helicity are displayed in Figures 2c and 2d. Helicity is important in dynamo action, particularly for inducing poloidal field from toroidal field [*Moffat*, 1978]. The sign of the helicity determines the

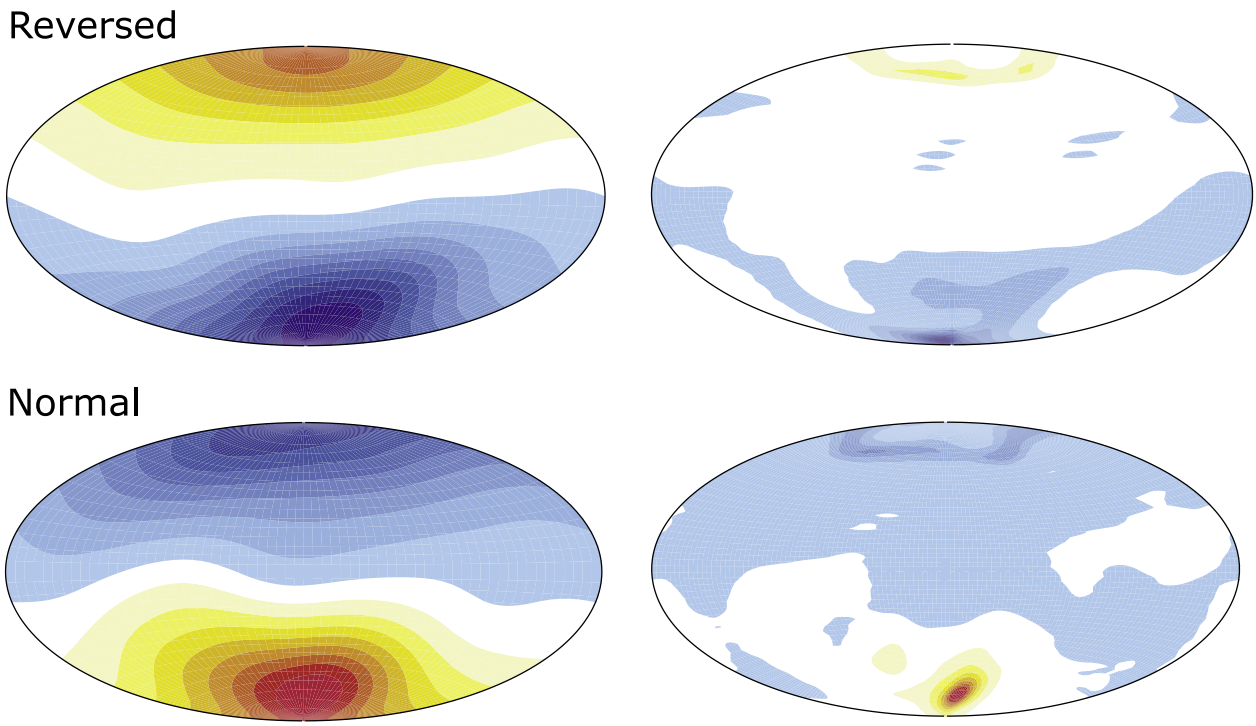

Figure 3. Radial magnetic field at a radial level representing the Earth's surface (left column) and at the outer boundary of the model (right column). Configurations show start (first row) and end (second row) of the standard reversal period shown as dark gray shaded area in Figure 1.

sign of the induced poloidal field, or alternatively, the direction of the induced toroidal electric currents relative to the direction of the toroidal magnetic field. Radial poloidal magnetic field, radial field production, the ϕ-component of the toroidal magnetic field, and helicity at times t_S and t_E are shown in Figures 4 and 5, respectively. The figures show south polar views at three different radii, $r_1 = r_o - 0.1$, $r_2 = r_i + 0.5$, and $r_3 = r_i + 0.1$, respectively, which represent radial surfaces in the outer core 10% away from the CMB, 10% away from the inner core and at mid-radius.

[36] The so called dynamo term in the dynamo equation (4) can be decomposed into a field production term and a field advection term:

$$\nabla \times (\mathbf{u} \times \mathbf{B}) = (\mathbf{B} \cdot \nabla)\,\mathbf{u} - (\mathbf{u} \cdot \nabla)\,\mathbf{B} \qquad (6)$$

Here, we have used the fact that magnetic and flow fields are divergence free. To visualize radial magnetic field production, we plot changes in the radial magnetic field due to the first term on the right hand side of equation (6) but neglect changes that are cancelled by the second term describing magnetic field advection. Below we will show an animation of azimuthal toroidal magnetic field advection, which displays changes of the field component due to the respective advective term in equation (6) but neglects changes that cancel with field production (See Animation 3).

[37] In the southern plumes, helicity is negative near the plume base and is positive near the top. This change in sign with height can be understood in terms of southern hemisphere quasi-geostrophic dynamics. Convergence in the upwelling near the base of the plume correlates with counterclockwise circulation, so helicity is negative there. Divergence near the plume top in combination with clockwise circulation results in positive helicity, but this positive helicity contributes only little to the overall poloidal field production which is much stronger deeper in the core. (Compare radial-field production in Figures 4 and 5.)

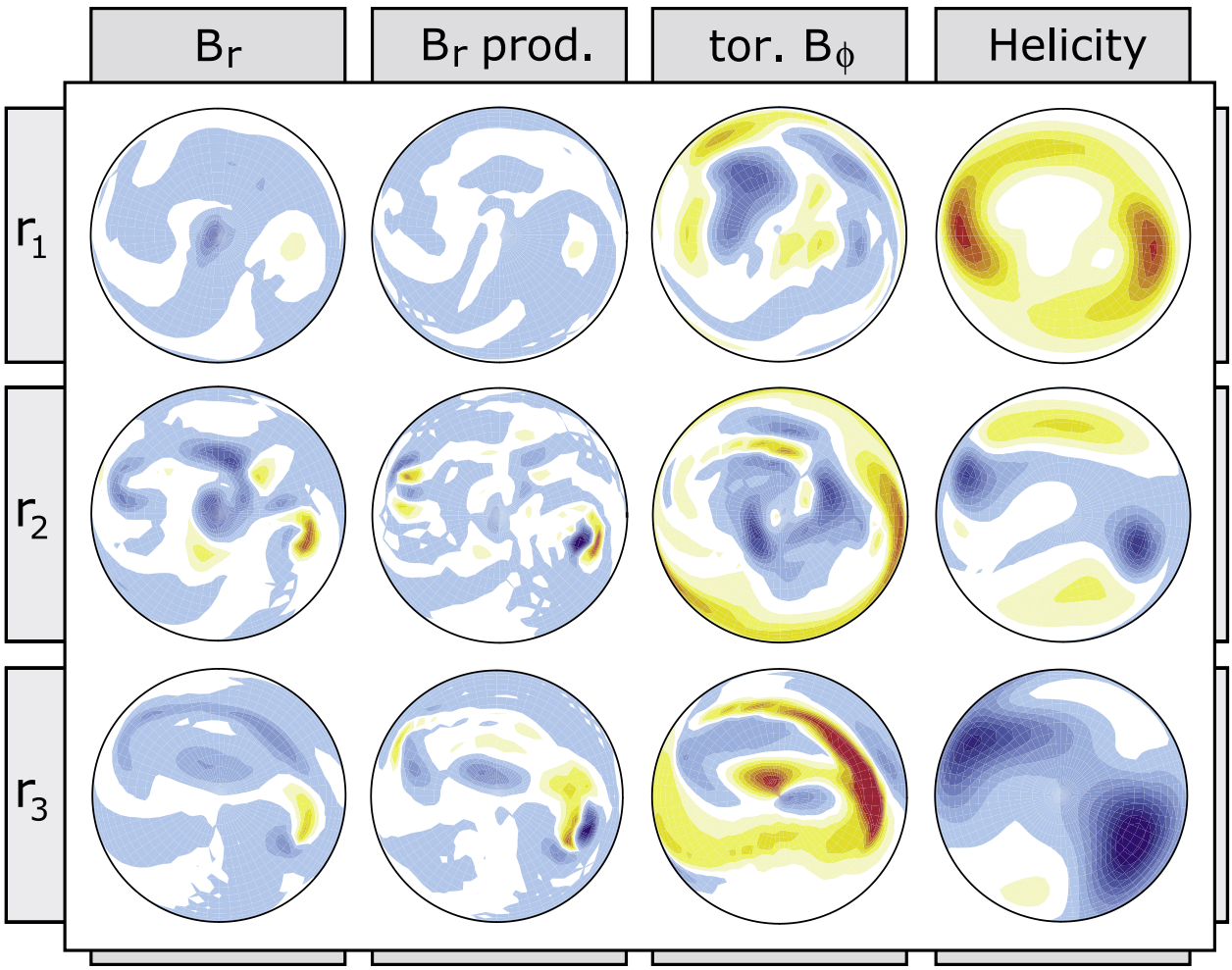

Figure 4. Radial magnetic field (first column), production of radial magnetic field (second column), ϕ-component of the toroidal field (third column), and helicity (fourth column) at three different radial levels in the outer core: $r_1 = r_o - 0.1$, $r_2 = r_i + 0.5$, and $r_3 = r_i + 0.1$ at the start of the reversal. The view is toward the south pole, and the same contour levels have been used at all radial levels. The dipole polarity radial field is reversed or negative (blue).

[38] The third important kinematic property of the plumes is their location relative to the meridional circulation. As shown in Figure 2, the northern polar plume is confined within the tangent cylinder region. Consequently it plays a secondary role in reversals. In contrast, the southern plumes are located outside the tangent cylinder on average, and are subject to the main meridional cell.

[39] Because the reversed field produced by these plumes is transported throughout the sphere by the main meridional cell, the interaction of the cell and the southern plumes plays a critical role in the timing and duration of the reversals. Indeed we find that the duration of the reversal of the external dipole is closely related to the south-to-north transport time in the meridional cell. Taken together, these three kinematic properties define this model as an $\alpha\omega m$-dynamo, the helical plumes providing the main α-effect, the azimuthal jets providing the main ω-effect, and the meridional circulation providing the m-effect. It is well established that $\alpha\omega m$-dynamos exhibit both ac (reversing) and dc (nonreversing) behavior, depending on the relative contributions of these three properties [*Moffat*, 1978]. However, our dynamo is not a classical $\alpha\omega m$-type, since the axisymmetric toroidal magnetic energy is only 20% of the total toroidal magnetic energy on average.

[40] Figures 4 and 5 reveal the complex details of the internal magnetic field generation. Selected 3-D

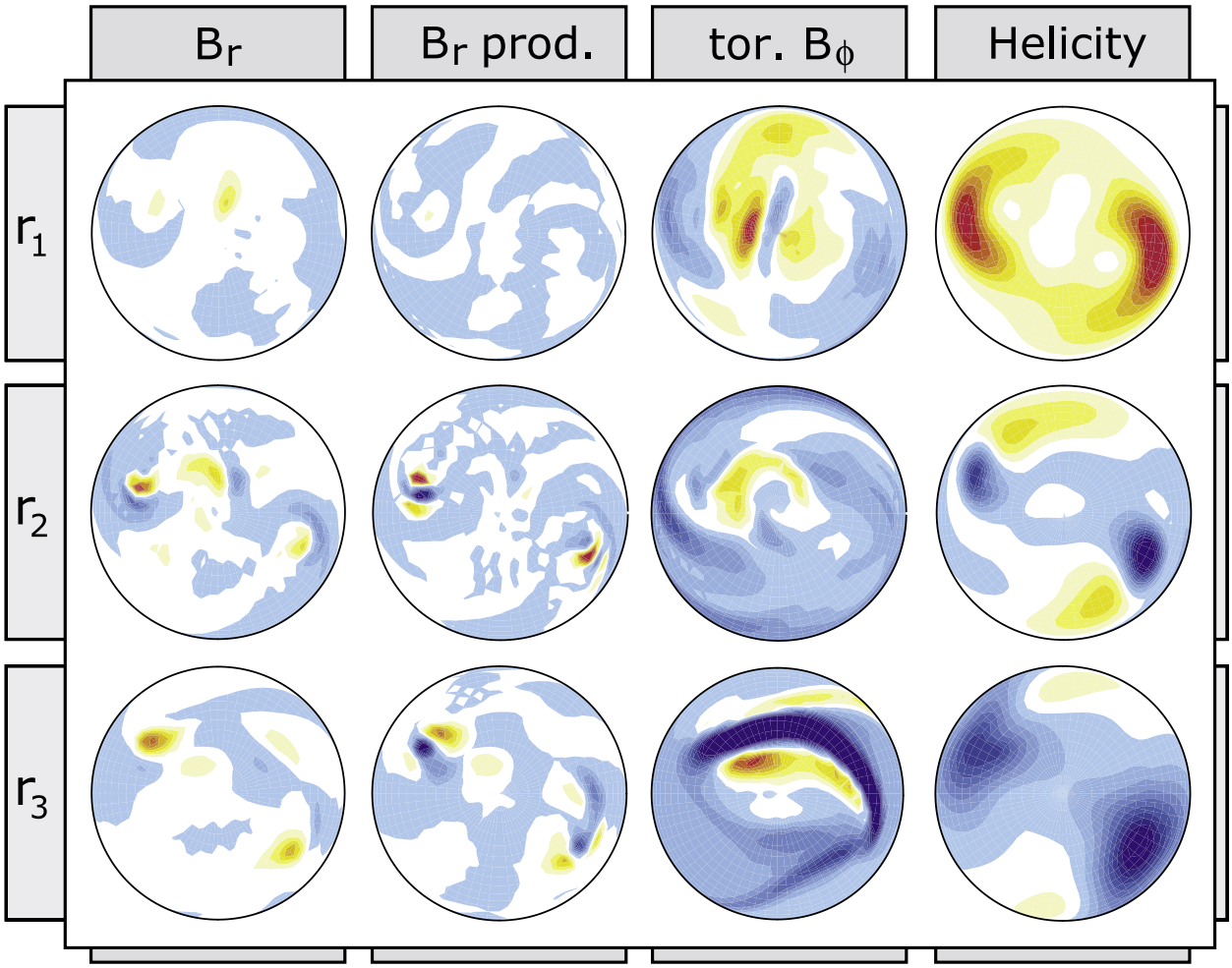

Figure 5. Same as Figure 4 but at the end of the standard reversal ($t = t_E$). The same contour levels have been used as in Figure 4. The dipole polarity radial field is now of normal polarity or positive (red).

fieldlines are shown in Figure 6 at t_S, the same time as in snapshots Figure 2, Figure 4, and the upper row of Figure 3. Helical motion associated with the rising plumes lifts and twists toroidal field to produce poloidal field loops. This action can most clearly be seen at the single plume in the northern hemisphere. Comparable effects are also seen in the southern hemisphere. Lifting of toroidal fieldlines by plumes creates radial field of both signs, and the resulting dipolar patches can be identified in Figures 4 and 5. Action of the strong plume helicity on the large toroidal field closer to the inner core is the most important source for inverse field. (See level r_3 in Figures 4 and 5.) Inverse field production has its maximum close to the plume center, but since normal polarity field is produced close by at the same time, there is significant cancellation which may retard the reversal process. In addition, there are also larger areas of inverse field production where weaker negative helicity outside the plume centers correlates with strong toroidal field. This is shown most convincingly at surface $r = r_3$ in Figure 4.

[41] The complexity in Figures 4 and 5 reveals the strong contribution of nonaxisymmetric toroidal field. Production of axisymmetric toroidal field by the classical Ω-effect is seen near the equator in Figure 6, for example. Advection plays an important role for the magnetic field dynamics in this dynamo and can even be stronger than field production due to the fast zonal flows. As men-

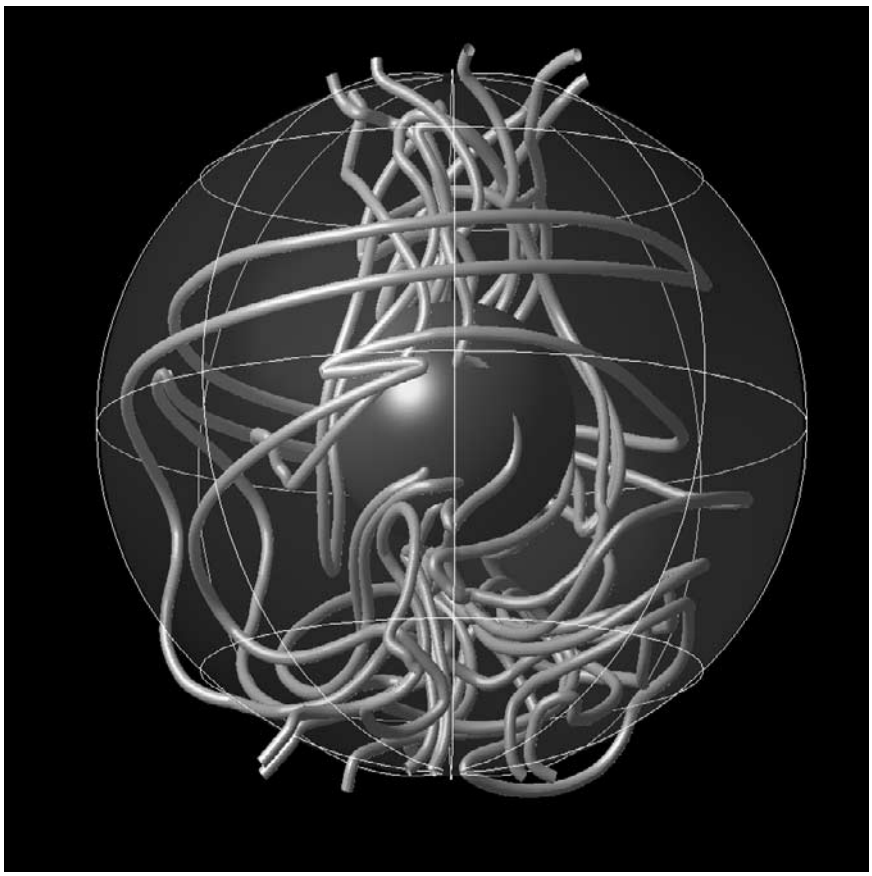

Figure 6. Three-dimensional configuration of selected internal magnetic field lines in the dynamo model at the start of the standard reversal.

tioned above, meridional transport distributes the reversed field from its source region to other parts of the core, and plays a crucial role in the reversal dynamics.

[42] Note the lack of equatorial symmetry in the snapshot images in Figures 2, 3, and 6. This asymmetry results from the internal dynamics of the system, and is not maintained by the boundary conditions, which are homogeneous in this calculation. Although hemispheric asymmetry persists over many dipole polarity epochs, it is not permanent. There is equal preference for a pattern in which the flow in the two hemispheres shown in these figures is reversed. Accordingly the long time-average flow pattern is expected to be symmetric and the average surface magnetic field is antisymmetric, with respect to the equator. However the flow pattern present during an individual polarity reversal is highly asymmetric, and is reflected in the asymmetric structure of the magnetic field during the transition period.

4.3. Reversal Dynamics

[43] To further explore the reversal dynamics, we have studied the time behavior of convective and magnetic fields in 2-D animations on various surfaces, as well as 3-D animations of isosurfaces. Animation 1 (available in the HTML version of the article at http://www.g-cubed.org) shows an animation of surface and axisymmetric magnetic fields over parts of three polarity epochs, including two successive polarity reversals (light gray shaded time interval in Figure 1). This animation includes the dipole polarity and relative dipole energy at the CMB, the radial field on the model boundary, the external field at a distance equivalent to Earth's surface, and the axisymmetric parts of the poloidal and toroidal fields. Animations 2

and 3 visualize the 3-D structure of the fields during the reversal period (dark gray shaded area in Figure 1). Animation 2 shows isosurfaces (positive and negative) of the poloidal magnetic field in z-direction and isosurfaces (positive and negative) of the helicity. Sequences of the axisymmetric fieldlines and CMB polarity are included to establish the position in the reversal process. The helicity animations show the motions of the northern and southern plumes.

[44] Finally, Animation 3 contains animations of isosurfaces of the toroidal magnetic field in ϕ-direction and isosurfaces of advection of this field component. The advection sequence demonstrates the importance of transport in the polarity transition process as seen at the CMB. Although the axisymmetric fields and isosurfaces help identify the most significant processes during the reversal, they must be complemented by 3-D views and cuts at different surfaces to fully depict the reversal process.

[45] The polarity reversal is most easily seen in the axisymmetric polodial field (fieldlines), where the sign of the azimuthal electric currents supporting this field have been color-coded. Sequences of this variable have therefore been included in all three animations. Examination of two different fieldline animations over three reversals confirms that the dynamics is always very similar from one reversal to the next. In each reversal, three stages can be distinguished; these are illustrated in Figure 7.

[46] The description below pertains to a reversal that starts from inverse polarity (outward radial dipole field in the northern hemisphere). This type of reversal is depicted in the 3-D animations and the first part of the 2-D animations above. The complement, a reversal from normal to inverse polarity, obeys the same dynamics and is shown in the second part of the 2-D animations. While the definitions of normal and reversed states are clear for the poloidal field, it is not so clear for the toroidal field. A possible definition of ''normal'' toroidal field would be the one produced from ''normal'' poloidal field. However, because the toroidal fields in this dynamo are typically complex, we mainly concentrate on the poloidal field in our analysis.

[47] 1. Polarity is inverse; reversal starts internally. In this initial stage the magnetic dipole at the CMB lies close to the geographic pole and its position is relatively stable. Seeds of stong normal polarity field are present in the interior, however. They can clearly be seen in the 3-D animations and as distortions in the axisymmetric fieldlines located at the downflow in the northern hemisphere and at the plume locations in the southern hemisphere. The magnetic energy grows while the helicity associated with the plumes and downflows in both hemispheres produces inverse as well as normal polarity field (See Figure 4 and Animation 2). Normal field appearing in the northern tangent cylinder causes the polarity to deviate farther from the 90° position and decreases the relative strength of the dipole at the CMB. Shearing of poloidal field by zonal flows creates toroidal field which is mainly retrograde in and near the northern tangent cylinder (see Animation 3), prograde at the equator (see Animation 3 and Figure 6), and more complex in the southern hemisphere (see Figure 4). This stage corresponds to Figures 7a and 7b.

[48] 2. Field reverses at the CMB. Normal radial field produced by plume action in the southern hemisphere is advected to the CMB in this stage, and marks the start of the reversal in the polarity function. The normal polarity field is then transported northward along the CMB by the meridional circulation. The polarity change at the CMB is completed when this advected field merges with the northern normal polarity patch. The advection and merging are evident in all animations of the axisymmetric fieldlines and can also be seen in the 3-D animation of toroidal magnetic field advection in (Animation 3). Stage 2 is represented by Figures 7b–7d.

[49] 3. Normal polarity consolidates. In addition to normal polarity field transported along the CMB, normal field produced in the northern tangent cylinder is also advected southward along the inner-core boundary. The remaining inverse polarity field cancels with the advected field and the locally produced normal polarity field. As a result, the magnetic energy decreases and field of mainly normal polarity remains. The ω-effect acting on the consolidated normal poloidal field produces toroi-

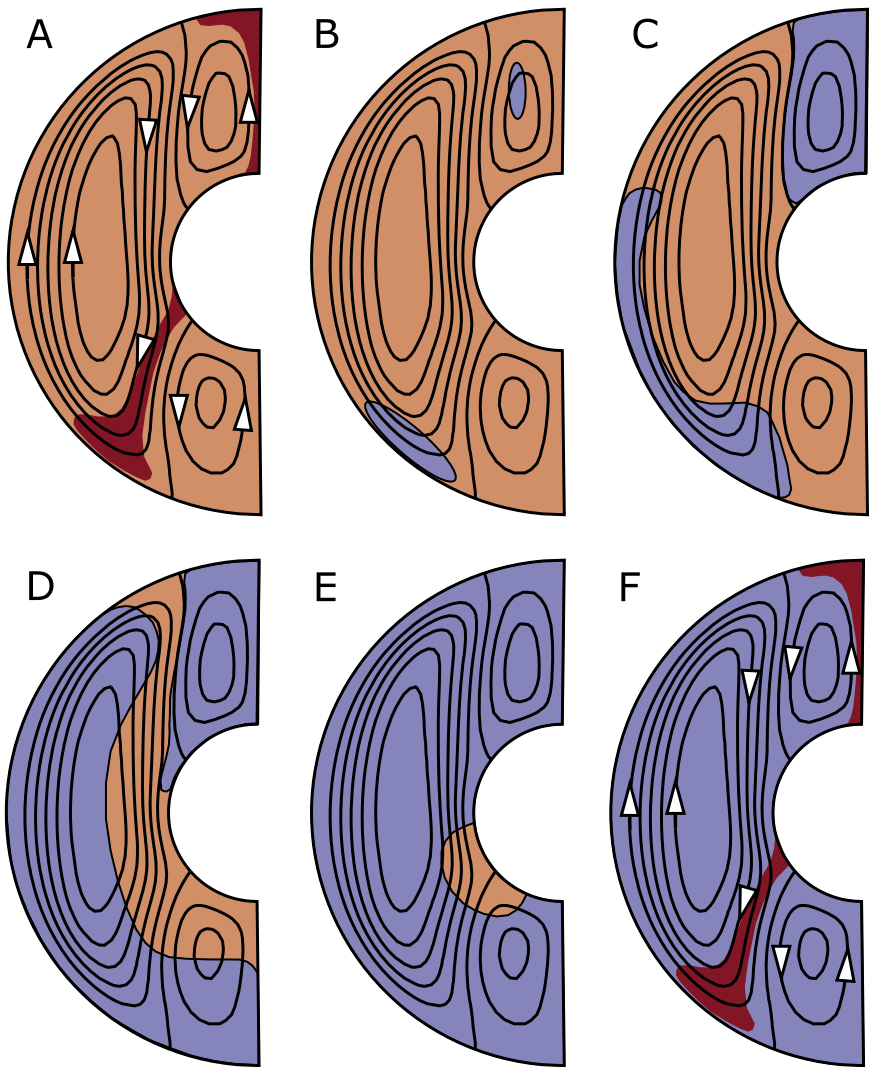

Figure 7. Sketch of the stages in a reversal sequence. Light red and light blue code the sign of the toroidal electric currents that produce the axisymmetric poloidal magnetic field. Contour lines are meridional streamlines. The first and last panels (a and f) show in addition directional arrows of the meridional circulation and plume locations (dark red).

dal field inverse to the starting configuration (see Animation 3). This toroidal field reversal close to the end of the sequence initializes the next reversal. Figures 7e–7f illustrate this stage.

5. Reversals in a Kinematic Dynamo Model

[50] Our interpretation of the reversal sequence does not appeal to any changes in the flow pattern to trigger the magnetic changes, and so is similar to a kinematic dynamo reversal. This begs the question: Are flow changes insignificant in the reversal process? To explore this question, we consider progressively simpler dynamo models. In a first simplification, the Lorentz force in the Navier-Stokes equation (1) is neglected (switched off in the code). Then the magnetic field does not affect the flow, and the velocity and buoyancy fields correspond to nonmagnetic convection.

[51] Figure 8 shows the resulting time sequences of such a simulation, over one magnetic diffusion time. This, and an equivalent calculation shown in Figure 1, start with identical (and self-consistent) initial conditions. There is a transient behavior when the flow adjusts to the new force balance

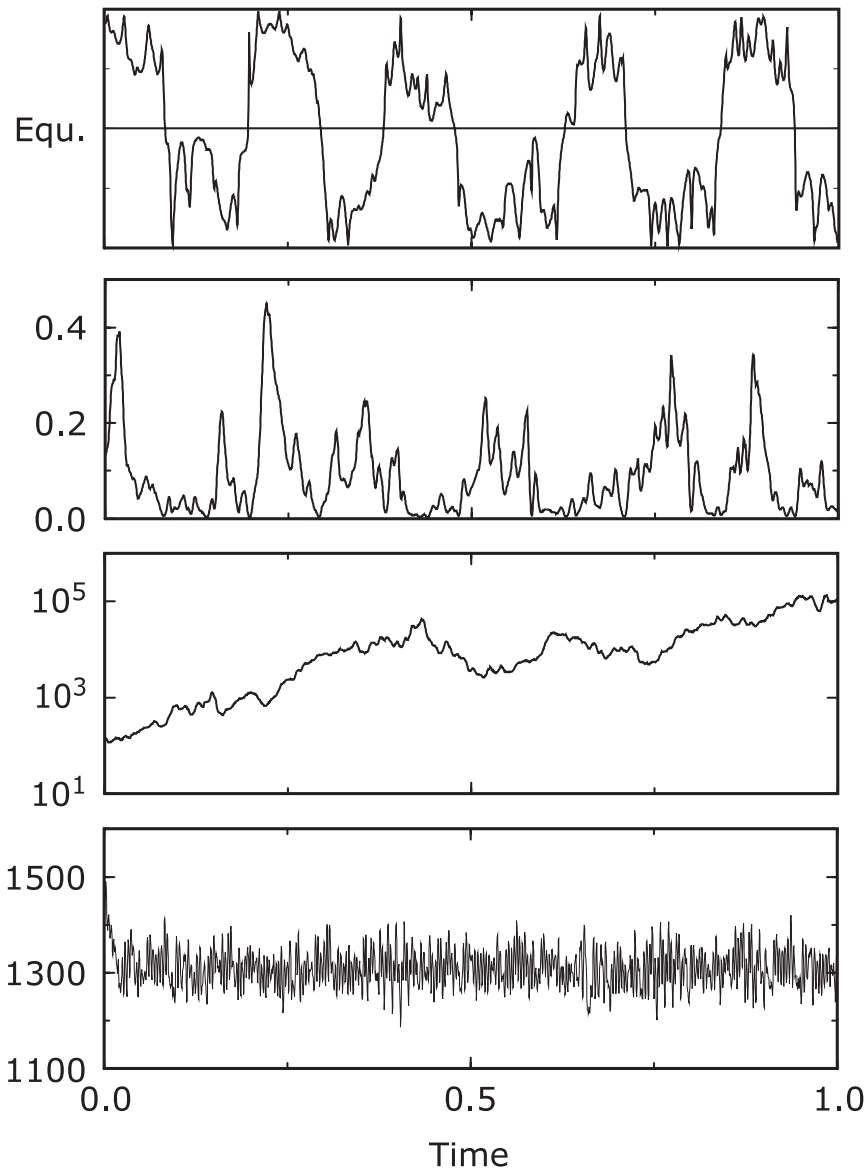

Figure 8. Time series of the dynamo model without Lorentz force. First panel shows dipole polarity function; second panel shows relative contribution of the magnetic dipole to the total magnetic energy at the CMB; third panel shows total magnetic energy in the outer core; fourth panel shows total kinetic energy. Compare this to the results for the full model in Figure 1.

(see kinetic energy in lower row of Figure 8). The dynamo without the Lorentz force still reverses, though somewhat more slowly, with 9 reversals during one magnetic diffusion time, versus 11 in the full model. This difference may be attributed to the chaotic nature of the solutions or the short duration of the run. The magnetic energy grows exponentially in time average due to the kinematic nature of this solution. An estimated growth rate is given in Table (1). The lower panel in Figure 8 shows the kinetic energy. The slow variation that was present in the self-consistent run (Figure 1) is largely gone in this case, demonstrating that this variation is an effect of magnetic back-reaction. Figure 9 compares shorter simulations, with and without the Lorentz force. The self-consistent case is the one depicted in Figure 1, while the run without the Lorentz force is the continuation of the simulation shown in Figure 8. The first panel in Figure 9 shows again the polarity function for orientation, and the second panel displays the magnetic energy density in the outer core (opposed

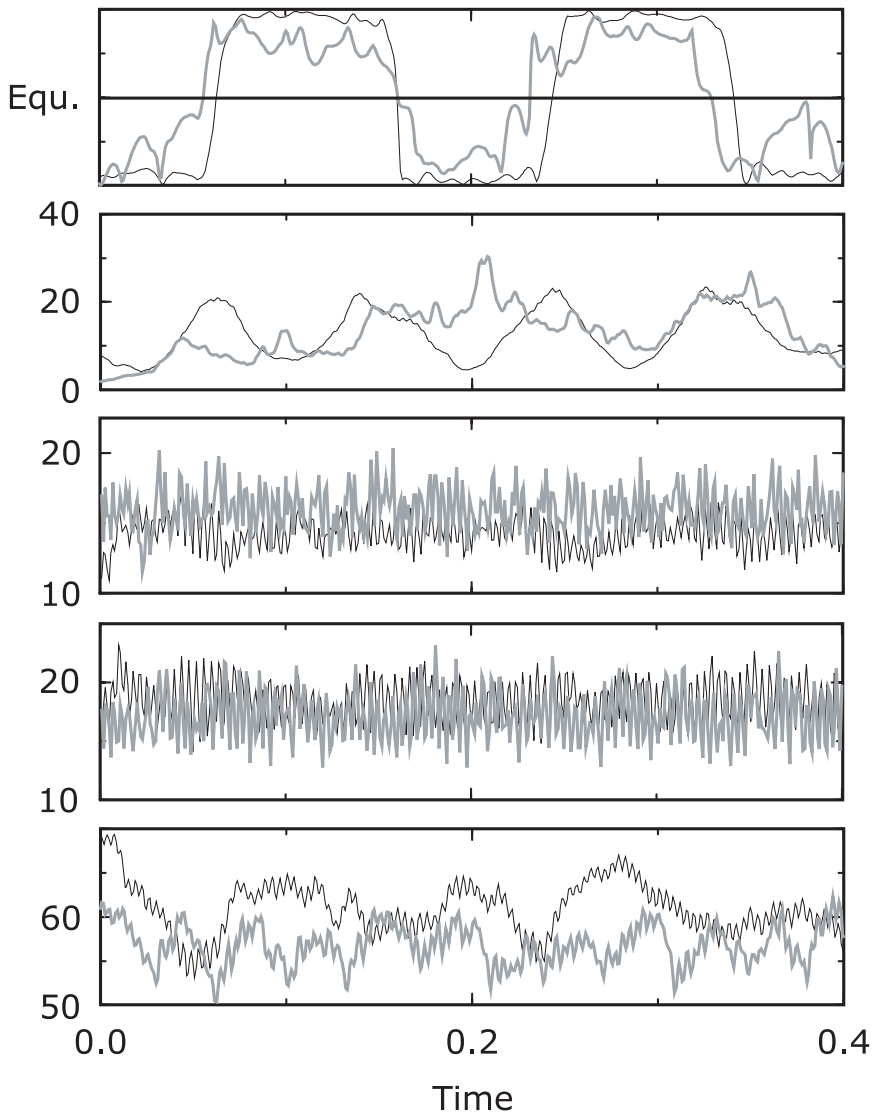

Figure 9. Comparison of two runs with (black lines) and without (gray lines) Lorentz force. First panel shows dipole polarity function; second panel shows magnetic energy density; third panel shows kinetic energy density of the flow through the radial surface at ($r = r_2$); fourth panel shows kinetic energy density of the flow through the equatorial plane; fifth panel shows kinetic energy density of zonal flow.

to total energy shown before). Panels three to five present additional flow measures: kinetic energy density of the flow through the radial surface at mid-radius (r_2) in row three, kinetic energy density of the flow through the equatorial plane in row four, and energy density of the zonal flow in row five. Two pronounced time scales can be distinguished: a fast convective time scale that we will describe in more detail below, and a slower magnetic time scale. In addition there are also intermediate convective time scales present. The slow magnetic time scale is most clearly recognizable in the zonal flow energy since poloidal magnetic field lines significantly impair zonal flow gradients.

[52] In the self-consistent case there is a good correlation between highs in magnetic energy and lows in kinetic energy. The opposite is true when the Lorentz force is neglected. In the latter case, the magnetic field strength more closely follows the intensity of convection. Since the magnetic field in the kinematic case is subject to the larger velocity

variations, it is significantly more time dependent, which complicates analysis of the reversal process. We nevertheless find the same overall dynamics as in the full system, and we therefore conclude that the Lorentz force has negligible influence on the reversal process in these models.

[53] In the full dynamo model, as in the convective calculation, the velocities exhibit a fast oscillation. This oscillation is related to the movement of the convective features in the northern hemisphere relative to their southern hemisphere counterparts. The relative rotation rate between the prograde northern and retrograde southern zonal motions is 4.6×10^4 degrees per magnetic diffusion time. This corresponds to an oscillation period of roughly 4×10^{-3} for the dominant $m = 2$ convective feature. At those times in the oscillation when hot regions in the northern hemisphere lie north of hot (cold) regions in the southern hemisphere the north-south meridional transport is suppressed (enhanced).

[54] Figure 10 illustrates these oscillations in various flow quantities: The first panel shows the kinetic energy density contained in different azimuthal wavenumbers. The axisymmetric energy (solid line) is varying only slightly while the oscillation is most pronounced in the $m = 2$ kinetic energy (long dashed line). The second panel shows the kinetic energy density of the flow through the radial surface midway between inner and outer boundary ($r = r_2$) for the northern hemisphere (solid line) and the southern hemisphere (dashed line). The convective flow is stronger in the south since two substantial upwellings are at work there compared to only one in the northern hemisphere. The main variation corresponds again to the ($m = 2$) oscillation, but fluctuations due to higher harmonics are also present. Panel three in Figure 10 demonstrates the substantial variations in the kinetic energy of the meridional flow through the equator. Finally, the lower panel of Figure 10 shows the variation in helicity, the solid line is the integrated helicity in the northern hemisphere, the dashed line is the respective value for the southern hemisphere. Though the variations are large in some of the flow components the integrated helicity changes very little.

[55] To further simplify the dynamo model, we have selected nine snapshots at times t_1 to t_9 in the principal convective oscillation as initial conditions for kinematic dynamo calculations. Gray lines mark t_1 to t_9 in Figure 10. Rather than solving an eigenvalue problem for the kinematic solution, we time-step the dynamo equations using steady-state velocity fields from snapshots t_1 to t_9. The most significant part of the convective dynamics missing from these calculations, labeled K_1 to K_9, is transport of convective features by the northern and southern zonal jets.

[56] The resulting polarity functions of the kinematic dynamo runs are shown in the left part of Figure 11. Note the transients that dominate each calculation until the largest growing eigenmode has taken over. Dynamos K_3 and K_8 reverse, while the other cases evolve into stationary eigen-solutions. For dynamo K_4 a stationary solution decays only slightly slower than an oscillatory eigenvector. Table 1 compares growth rates and reversing periods for all dynamos presented in this paper. Most stationary kinematic dynamos have a large positive growth rate, while K_3 and K_4 decay. The growth rates of K_8 and K_9 are positive, but smaller than for the other stationary cases. The reversal rate is slower than in the self-consistent case, about 6 reversals per magnetic diffusion time for dynamo K_3 and nearly 7 reversals per magnetic diffusion time for dynamo K_8.

[57] Figure 12 shows the radial magnetic field at mid radius r_2 for a normal polarity situation and an intermediate state of dynamo K_3. The action of the central northern plumes and two large plus one smaller upwellings in the southern hemisphere can again be identified. In the intermediate configuration the southern hemisphere has mainly reversed, but the northern hemisphere has reversed only partially. This configuration is similar to the stationary eigensolution found for most of the other kinematic cases.

[58] Surprisingly, dynamo K_3 oscillates, while dynamo K_7 is stationary, even though the two convective fields are very similar (see Figure 10). We have not identified reasons for this difference in behavior. Perhaps subtle differences in the velocity

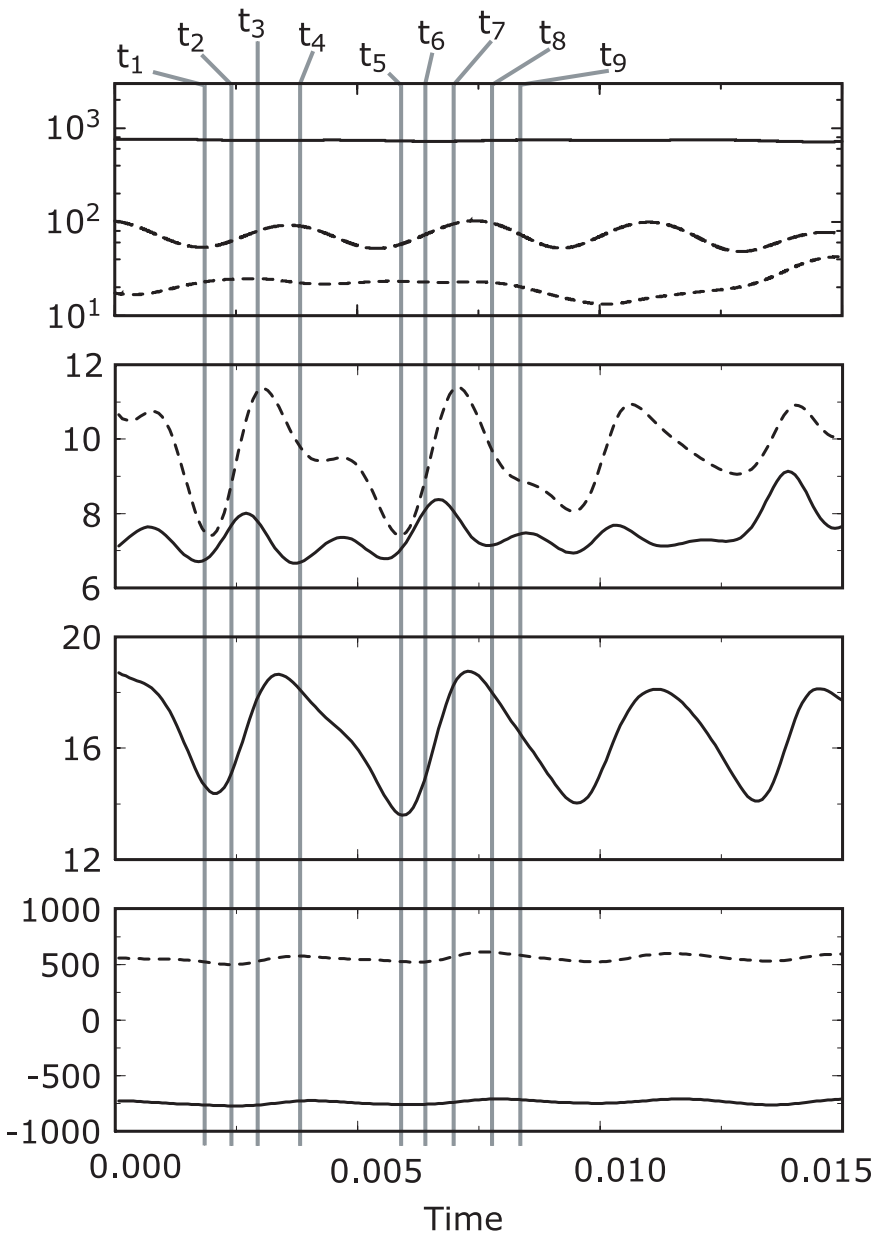

Figure 10. Time sequence of different flow quantities that demonstrate the fast convective oscillations: Upper panel shows kinetic energy density for different wave numbers, solid, axisymmetric; short dashed, (m = 1); long dashed, (m = 2). Second panel shows kinetic energy density of the flow through the radial plane at mid radius between inner and outer boundary, solid, northern hemisphere; dashed, southern hemisphere. Third panel shows kinetic energy density of the flow through the equatorial plane. Lower panel shows mean helicity density, solid, northern hemisphere, dashed, southern hemisphere. The vertical gray lines mark times where snap shots of the flow field have been used for kinematic dynamo simulations (see Figure 11).

field suffice to determine whether the growth rate of an oscillatory or a stationary solution is largest. It is tempting to conclude that the meridional circulation is a determining feature, since the two oscillating dynamos K_3 and K_8 are based on convective solutions with large flows across the equatorial plane. This agrees with our finding that meridional circulation is important for the reversal in the self-consistent case. On the other hand, the flow across the equatorial plane is as

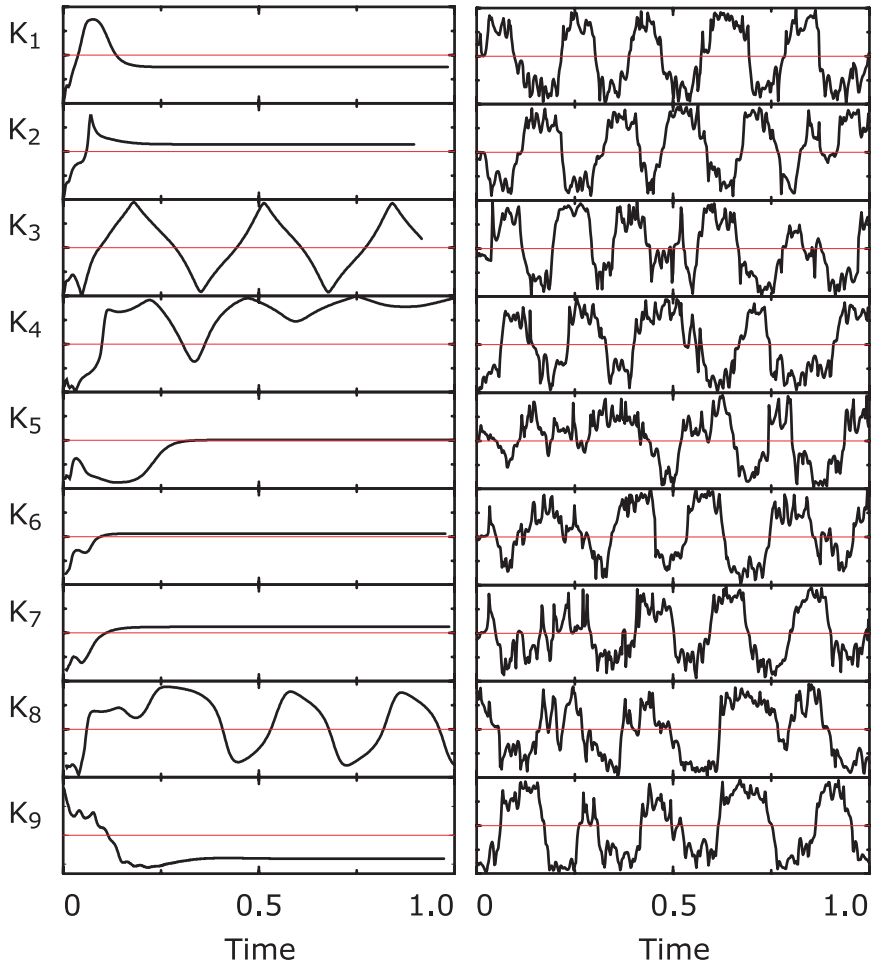

Figure 11. The left part shows kinematic dynamo simulations for nine different velocity fields taken from snapshots t_1 to t_9 of the run shown in Figure 10. The curves show the colatitude of the dipole component at the core-mantle boundary, thin horizontal lines mark the equator. Note how the fastest growing eigenmodes take over after a transient. For the right part we have used the end configurations of the kinematic runs as starting solutions for a dynamic calculation without Lorentz force (See Figure 8).

large for the stationary solution K_7 as for the oscillating cases.

[59] Additional numerical simulations confirm that stationary eigensolutions dominate the kinematic dynamo cases. However, model runs without Lorentz force reverse with rates similar as in the selfconsistent case and in kinematic dynamos K_3 and K_8. It seems that the grothrates found in the kinematic solutions do not reflect to behavior of the dynamically evolving system. Note that the time scale of the flow oscillations is two orders of magnitude smaller than the reversal periods and is also much smaller than the typical kinematic growth times. This suggests that stationary velocity fields may indeed not reflect the correct temporal

Table 1. List of Growth Rates and Time Behavior for the Dynamo Simulations Presented Here: The Self-Consistent Case, a Run Without Lorentz Force and Nine Kinematic Calculations K_1 to K_9[a]

Name	Growth Rate	Period
Self-consistent	Equilibrated	≈0.09
No Lorentz-force	≈6	≈0.11
K_1	61.2	Stationary
K_2	55.1	Stationary
K_3	−2.1	0.16
K_4	≈−10	Stationary (0.12)
K_5	30.2	Stationary
K_6	89.1	Stationary
K_7	53.1	Stationary
K_8	5.4	0.14
K_9	8.5	Stationary

[a] For dynamo K_4 an oscillating and a stationary eigensolution have about the same decay rate, the stationary solution decaying somewhat slower. This complicated the determination of growth rate and period.

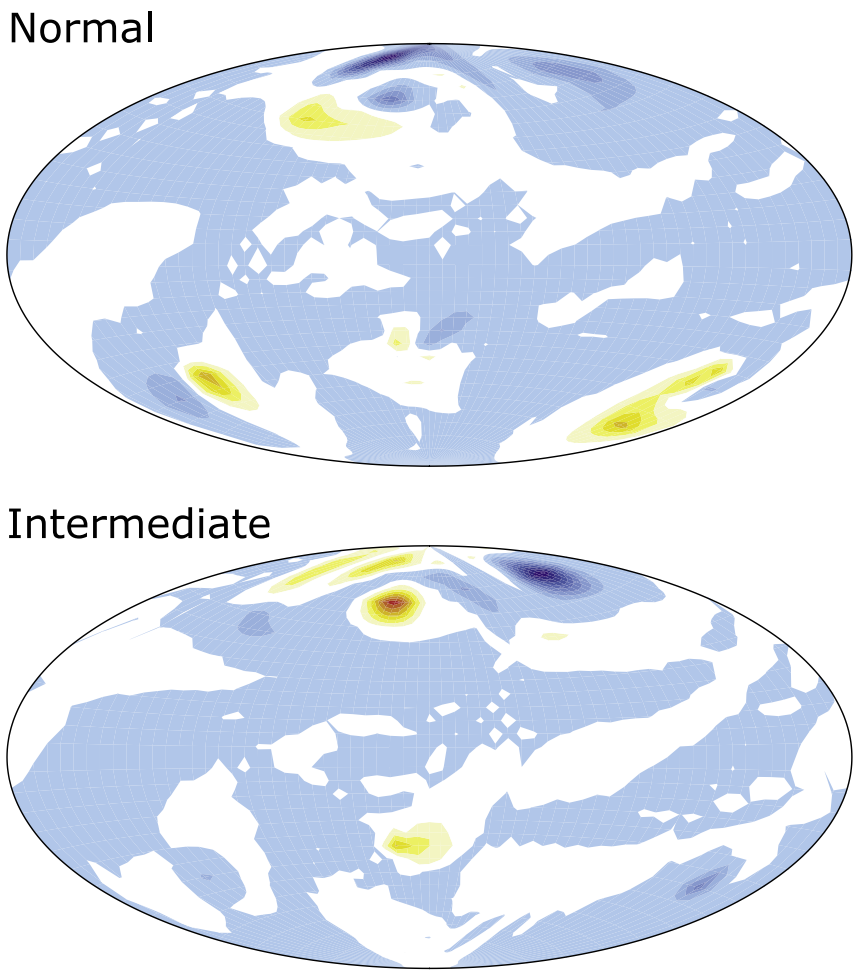

Figure 12. Radial magnetic field structure at normal and intermediate polarity of kinematic dynamo K_3.

behavior. We have conducted additional numerical experiments, using the end configurates of the kinematic dynamo runs K_1–K_9 as starting solutions for respective integrations without Lorentz forces. The results are shown in the right part of Figure 11. Most of the stationary solutions resume to reverse after a time span shorter than the reversal period. Clearly, oscillatory solutions are prefered for all starting conditions, and this preference is a consequence of the dynamical changes in the convective flow.

[60] We conclude that our self-consistent dynamic dynamo model is close to being kinematic in its overall behavior because the Lorentz force is not essential for the reversals to happen and because similar oscillatory kinematic solutions can be found. Moreover, it is unlikely that the reversals are initiated by any particular changes in the flow, since the typical convective oscillation period is so much smaller than the reversal period. The reversals are therefore pure magnetic modes intrinsic to the dynamo.

[61] It is commonly thought that Lorentz forces play a much more significant role in the Earth's outer core than in the model reported here and than in possibly all dynamo simulations to date [*Hollerbach*, 1996; *Jones*, 2000]. The geomagnetic field is therefore probably far from any kinematic solution. What this means for the reversal rate and the reversal mechanism itself remains to be explored.

6. Summary

[62] The dynamo model presented here undergoes regular, nearly periodic reversals, with uniform

polarity epochs separated by brief dipole polarity transitions. It approximates an $\alpha\omega m$-type dynamo, with helical convective plumes (α-effect), azimuthal jets (ω effect) and meridional circulation (m-effect). The dynamo is "nearly kinematic" due to the large magnetic Roberts number employed ($q = 20$). Fluctuations in the magnetic field, including the polarity reversals, are far larger than fluctuations in the velocity field.

[63] Viewed from outside, the dipole reversal "starts" when upwelling plumes twist toroidal field, producing spots with reversed poloidal field near the outer boundary. Accordingly, reversed flux spots on the outer boundary above the plumes are precursors to the dipole reversal. The reversed poloidal field is advected northward from the southern plumes by the meridional circulation. This determines the transition time, and corresponds to a few thousand years in the Earth's core. Because the meridional circulation crosses the equator, the transitional field on the outer boundary is quadrupolar. The reversal "finishes" with an inversion of the toroidal magnetic field in the southern hemisphere, which in turn initiates the next poloidal field reversal. From outside, the reversal occurs in a fraction of the time needed to complete the reversal process throughout the core. Similar mechanisms may be at work in reversals of the geodynamo.

[64] The duration of polarity epochs is more difficult to link to a single dynamical process. In general terms, the duration of a polarity epoch represents a sort of "mixing time" for the poloidal and toroidal magnetic field scalars P and τ. It depends on multiple effects, including the relative strengths of the reversed and normal fields produced in the plumes, meridional flux advection, and flux diffusion. The polarity epochs in our model are short, equivalent to about 25 kyr in the core.

[65] Although the meridional circulation in our model promotes reversals, several kinematic dynamo calculations show the opposite effect, that meridional circulation can suppress oscillatory solutions in favor of stationary ones [*Roberts*, 1972; *Sarson and Gubbins*, 1996]. An explanation for this discrepancy could be the direction of the meridional transport. The meridional circulation in our models transports disturbances from the southern hemisphere across the equator, and is also relatively strong. In contrast, the kinematic dynamo simulations by *Roberts* [1972] and *Sarson and Gubbins* [1996] assume equatorial antisymmetric meridional cells, which tend to confine disturbances to one hemisphere.

[66] This interpretation offers a way to reconcile the results of *Sarson and Jones* [1999] with ours. Since reversals in their dynamo model begin when the meridional circulation is especially weak, *Sarson and Jones* [1999] concluded that low meridional flow enables the reversal to start. However, during the reversal itself, the meridional flow in their model crosses the equator and actually increases in strength (see panels 2, 3 and 4 in Figure 4 of *Sarson and Jones* [1999]), more like the meridional flow in our models.

[67] We find that meridional transport plays a key role in determining the frequency and duration of reversals. Subtle differences in meridional transport can account for many of the differences seen in dynamo model reversals, and may possibly account for differences between reversals in the paleomagnetic record.

Acknowledgments

[68] This research has been supported by a grant to Peter Olson from the Geophysics Program of the National Science Foundation and by the Priority Program "Geomagnetic Variations" of the Deutsche Forschungsgemeinschaft. Special thanks goes to Julien Aubert for cooking some very tasty fieldline pasta for us (Figure 6).

References

Bloxham, J., D. Gubbins, and A. Jackson (1989), Geomagnetic secular variation, *Philos. Trans. R. Soc. London*, *A329*, 415–502.

Cande, S., and D. Kent (1995), Revised calibration of the geomagnetic polarity timescales for the late cretaceous and cenozoic, *Geophys. Res. Lett.*, *100*, 6093–6095.

Christensen, U., P. Olson, and G. Glatzmaier (1999), Numerical modeling of the geodynamo: A systematic parameter study, *Geophys. J. Int.*, *138*, 393–409.

Coe, R., L. Hongre, and A. Glatzmaier (2000), An examination of simulated geomagnetic reversals from a paleomagnetic perspective, *Philos. Trans. R. Soc. London*, *A358*, 1141–1170.

Constable, G. (2000), On the rate of occurence of geomagnetic reversals, *Phys. Earth Planet. Inter.*, *118*, 181–193.

Cox, A. (1975), Reversed flux as reversal mechanism, *Rev. Geophys. Space Phys.*, *13*, 35–51.

Dormy, E., J.-P. Valet, and V. Courtillot (2000), Numerical models of the geodynamo and observational constraint, *Geochem. Geophys. Geosys.*, *1*, Paper number 2000GC0000062.

Glatzmaier, G. (1984), Numerical simulation of stellar convective dynamos: 1. The model and methods, *J. Comput. Phys.*, *55*, 461–484.

Glatzmaier, G., and P. Roberts (1995), A three-dimensional convective dynamo solution with rotating and finitely conducting inner core and mantle, *Phys. Earth Planet. Inter.*, *91*, 63–75.

Glatzmaier, G., R. Coe, L. Hongre, and P. Roberts (1999), The role of the Earth's mantle in controlling the frequency of geomagnetic reversals, *Nature*, *401*, 885–890.

Grote, E., and F. Busse (2000), Hemispherical dynamos generated by convection in rotating spherical shells, *Phys. Rev.*, *62*, 4457–4460.

Gubbins, D. (1987), Mechanism for geomagnetic polarity reversals, *Nature*, *326*, 167–169.

Gubbins, D. (1999), The distinction between geomagnetic excursions and reversals, *Geophys. J. Int.*, *137*, F1–F3.

Harland, W., R. Armstrong, A. Cox, L. Craig, A. Smith, and D. Smith (1990), *A Geological Time Scale*, Cambridge Univ. Press, New York.

Hollerbach, R. (1996), On the theory of the geodynamo, *Phys. Earth Planet. Inter.*, *98*, 163–185.

Hollerbach, R., and C. Jones (1993), Influence of the Earth's inner core on the geomagnetic fluctuations and reversals, *Nature*, *365*, 541–543.

Hulot, G., C. Eymin, B. Langlais, M. Mandea, and N. Olson (2002), Small-scale structure of the geodynamo inferred from Oersted and Magsat satellite data, *Nature*, *416*, 620–623.

Jackson, A., A. Jonkers, and M. Walker (2000), Four centuries of geomagnetic secular variation from historical records, *Philos. Trans. R. Soc. London*, *A358*, 957–990.

Jacobs, J. (Ed.) (1984), *Reversals of the Earth's Magnetic Field*, Adam Hilger, Bristol.

Jones, C. A. (2000), Convection-driven geodynamo models, *Philos. Trans. R. Soc. London*, *A358*, 873–897.

Kageyama, A., M. Ochi, and T. Sato (1999), Flip-flop transition of the magnetic intensity and polarity reversals in the magnetohydrodynamic dynamo, *Phys. Rev. Lett.*, *82*, 5409–5412.

Kida, S., K. Araki, and H. Kitauchi (1997), Periodic reversals of magnetic field generated by thermal convection in a rotating spherical shell, *J. Phys. Soc. Jpn.*, *66*, 2194–2201.

Kono, M., and P. Roberts (2002), Recent geodynamo simulations and observations of the geomagnetic field, *Rev. Geophys.*, *40*, 1013, doi:10.1029/2000RG000102.

Kutzner, C., and U. Christensen (2002), From stable dipolar to reversing numerical dynamos, *Phys. Earth Planet. Inter.*, *131*, 29–45.

Langereis, C., M. Dekkers, G. de Lange, M. Paterne, and P. van Santvoort (1997), Magnetostratigraphy and astronomical calibration of the last 1.1 myr from an eastern Mediterranean piston core and dating of short events in the brunes, *Geophys. J. Int.*, *129*, 75–94.

Merrill, R., and P. McFadden (1999), Geomagnetic polarity transitions, *Rev. Geophys.*, *37*, 201–226.

Merrill, R., M. McElhinny, and P. McFadden (1996), *The Magnetic Field of the Earth*, Academic, San Diego, Calif.

Moffat, H. (1978), *Magnetic Field Generation in Electrically Conducting Fluids*, Cambridge Univ. Press, New York.

Roberts, P. (1972), Kinematic dynamo models, *Philos. Trans. R. Soc. London*, *A271*, 663–697.

Sarson, G., and D. Gubbins (1996), Three-dmensional kinematic dynamos dominated by strong differential rotation, *J. Fluid Mech.*, *306*, 223–265.

Sarson, G., and C. Jones (1999), A convection driven geodynamo reversal model, *Phys. Earth Planet. Inter.*, *111*, 3–20.

Secco, R., and H. Schloessin (1989), The electrical resistivity of solid and liquid fe at pressures up to 7 gpa, *J. Geophys. Res.*, *94*, 5887–5894.

Valet, J.-P., and L. Meynadier (1993), Geomagnetic field intensity and reversals during the past four million years, *Nature*, *366*, 234–238.

Wicht, J. (2002), Inner-core conductivity in numerical dynamo simulations, *Phys. Earth Planet. Inter.*, *132*, 281–302.